the FEBS Journal

Towards a functional identification of catalytically inactive [Fe]-hydrogenase paralogs

Takashi Fujishiro[1], Kenichi Ataka[2], Ulrich Ermler[3] and Seigo Shima[1,4]

1 Max-Planck-Institut für terrestrische Mikrobiologie, Marburg, Germany
2 Department of Physics, Freie Universität Berlin, Germany
3 Max-Planck-Institut für Biophysik, Frankfurt/Main, Germany
4 PRESTO, Japan Science and Technology Agency (JST), Saitama, Japan

Keywords
[Fe]-hydrogenase; Hmd paralogs; methanogenic archaea; sensor protein; tetrahydromethanopterin

Correspondence
S. Shima, Max-Planck-Institut für terrestrische Mikrobiologie, Karl-von-Frisch-Straße 10, 35043 Marburg, Germany
Fax: +49 6421 178199
Tel: +49 6421 178122
E-mail: shima@mpi-marburg.mpg.de

(Received 20 April 2015, revised 15 June 2015, accepted 17 June 2015)

doi:10.1111/febs.13351

[Fe]-hydrogenase (Hmd), an enzyme of the methanogenic energy metabolism, harbors an iron-guanylylpyridinol (FeGP) cofactor used for H_2 cleavage. The generated hydride is transferred to methenyl-tetrahydromethanopterin (methenyl-H_4MPT^+). Most hydrogenotrophic methanogens contain the *hmd*-related genes *hmdII* and *hmdIII*. Their function is still elusive. We were able to reconstitute the HmdII holoenzyme of *Methanocaldococcus jannaschii* with recombinantly produced apoenzyme and the FeGP cofactor, which is a prerequisite for *in vitro* functional analysis. Infrared spectroscopic and X-ray structural data clearly indicated binding of the FeGP cofactor. Methylene-H_4MPT binding was detectable in the significantly altered infrared spectra of the HmdII holoenzyme and in the HmdII apoenzyme–methylene-H_4MPT complex structure. The related binding mode of the FeGP cofactor and methenyl-H_4MPT^+ compared with Hmd and their multiple contacts to the polypeptide highly suggest a biological role in HmdII. However, holo-HmdII did not catalyze the Hmd reaction, not even in a single turnover process, as demonstrated by kinetic measurements. The found inactivity can be rationalized by an increased contact area between the C- and N-terminal folding units in HmdII compared with in Hmd, which impairs the catalytically necessary open-to-close transition, and by an exchange of a crucial histidine to a tyrosine. Mainly based on the presented data, a function of HmdII as Hmd isoenzyme, H_2 sensor, FeGP-cofactor storage protein and scaffold protein for FeGP-cofactor biosynthesis could be excluded. Inspired by the recently found binding of HmdII to aminoacyl-tRNA synthetases and tRNA, we tentatively consider HmdII as a regulatory protein for protein synthesis that senses the intracellular methylene-H_4MPT concentration.

Database
Structural data are available in the Protein Data Bank under the accession numbers 4YT8; 4YT2; 4YT4 and 4YT5.

Abbreviations
apo-Hmd, Hmd apoenzyme; apo-HmdII, HmdII apoenzyme; C-unit, central globular unit; FeGP, iron-guanylylpyridinol; H_4MPT, tetrahydromethanopterin; holo-Hmd, Hmd holoenzyme reconstituted with the FeGP cofactor; holo-HmdII, HmdII holoenzyme reconstituted with the FeGP cofactor; N-unit, N-terminal domain unit; SeMet, L-selemomethionine.

Introduction

[Fe]-hydrogenase, also known as H_2-forming methylene-tetrahydromethanopterin (methylene-H_4MPT) dehydrogenase (Hmd), is one of three known hydrogenases [1–5]. Hmd is involved in the methanogenic pathway of many hydrogenotrophic methanogenic archaea and reversibly catalyzes the stereoselective hydrogenation of methenyl-H_4MPT^+ to methylene-H_4MPT using H_2 as a hydride donor (Fig. 1A) [6,7].

Hmd occurs as a homodimer consisting of a central globular unit (termed C-unit) formed by the C-terminal domains of each subunit and two N-terminal Rossmann-like domains (termed N-unit). Hmd was found in an 'open' or 'closed' conformation [3], defined by the orientation of the C- and N-units relative to each other. The active site is located between them and the open-to-close transition is considered to play a crucial role in the catalytic cycle [2,6]. Each N-unit of Hmd harbors one iron-guanylylpyridinol (FeGP) cofactor as a prosthetic group (Fig. 1B) [4,8]. The iron center is coordinated by two *cis*-CO, one cysteine-thiolate, one solvent, and the pyridinol-nitrogen and the acyl-carbon of the guanylylpyridinol ligand [9–13]. Based on the X-ray crystal structure of Hmd complexed with isocyanide inhibitors, the solvent-binding site of the organometallic iron–carbonyl complex has been proposed to serve as the H_2-binding site [14,15]. The FeGP cofactor can be extracted from the Hmd holoenzyme (holo-Hmd) [13,16] and subsequently used to reconstitute a fully active holo-Hmd from an Hmd apoenzyme (apo-Hmd). The X-ray structure of the reconstituted holo-Hmd of *Methanocaldococcus jannaschii* revealed binding of the intact FeGP cofactor [1,2,4].

The genomes of many hydrogenotrophic methanogenic archaea harbor genes related to the *hmd* gene. The encoding proteins HmdII and HmdIII have 20–30% amino acid sequence identity with Hmd [17]; those of *M. jannaschii* (HmdII, MJ1338 and HmdIII, MJ0715) show ~ 20% identity to Hmd (MJ0784) [18]. Some hydrogenotrophic methanogens, e.g. *Methanococcus voltae* (US DOE Joint Genome Institute, Walnut Creek, CA, USA) and *Methanobrevibacter smithii* [19], have an *hmd* gene and produce active Hmd [20] but their genomes do not harbor genes encoding HmdII and HmdIII. The *hmdII* gene has been recently identified in the genome of the hyperthermophilic bacterium *Desulfurobacterium thermolithotrophum*, but this non-methanogen lacks the *hmd* gene [21].

HmdII and HmdIII from various methanogens have a sequence identity of ~ 60–80% relative to each other (those from *M. jannaschii* 65%), which indicates that HmdII and HmdIII have similar structures and functions. After their identification in genomes, HmdII and HmdIII were tentatively considered as Hmd homologs that catalyze the same reaction as Hmd [22]. Later on, preliminary data suggested that HmdII can bind the FeGP cofactor [23,24]; however, neither HmdII nor HmdIII have been reconstituted with the FeGP cofactor and kinetically analyzed. Therefore, their function remains elusive.

Here, we present the reconstitution of the HmdII holoenzyme (holo-HmdII) from the HmdII apoenzyme (apo-HmdII) and the FeGP cofactor, its infrared spectroscopic characterization, kinetic studies and X-ray structure analysis of the apo-HmdII, holo-HmdII and apo-HmdII with bound methylene-H_4MPT. Based on the obtained results, we discuss potential functions of the Hmd-related proteins.

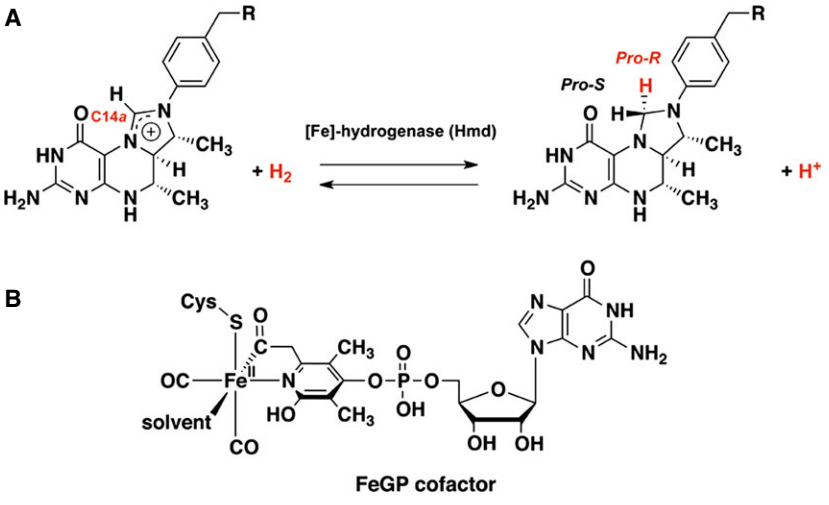

Fig. 1. Hmd-catalyzed reaction and structure of the FeGP cofactor. (A) Hmd-catalyzed reversible hydrogenation of methenyl-H_4MPT^+. **R** indicates the residual part of the H_4MPT derivative. (B) Chemical structure of the FeGP cofactor. Upon reaction, H_2 replaces the solvent at the FeGP cofactor iron, is heterolytically cleaved, and the generated hydride is subsequently transferred from the *pro-R* side to the carbocationic C14*a* of methenyl-H_4MPT^+ [7].

Results

Infrared analysis of holo-HmdII

In the infrared spectrum of holo-HmdII, the peaks of the antisymmetric and symmetric stretching band of the iron-ligating CO were split and have frequencies of 2015 + 1994 cm^{-1} and 1946 + 1930 cm^{-1}, respectively (Fig. 2). These frequencies resembled those of holo-Hmd (2011 and 1944 cm^{-1}), which is indicative of similar environments for the iron complexes. The peak splitting argued for at least two distinct FeGP-binding modes. Addition of methylene-H_4MPT to the holo-HmdII solution resulted in a minor frequency shift and a substantial intensity change of the CO bands (Fig. 2). Moreover, the CO peaks are sharper in holo-HmdII than in holo-Hmd, implying that the CO ligands are more encapsulated after binding methylene-H_4MPT. By contrast, methenyl-H_4MPT^+ changed the infrared spectrum of holo-HmdII only slightly, but appears also to bind in the vicinity of the CO ligands. The greater influence of methylene-H_4MPT on the environment of CO might reflect larger conformational changes of the protein.

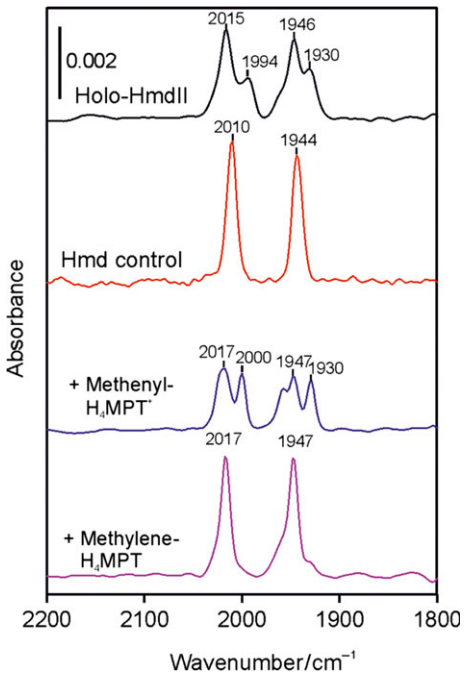

Fig. 2. Infrared spectra of holo-HmdII and holo-Hmd. Black line, holo-HmdII; red line, holo-Hmd; blue line, holo-HmdII in the presence of methenyl-H_4MPT^+; magenta line, holo-HmdII in the presence of methylene-H_4MPT.

X-Ray structure analysis of HmdII of *Methanocaldococcus jannaschii*

Overall structure

The crystal structures of apo-HmdII and reconstituted holo-HmdII from *M. jannaschii* have been determined at 1.9 and 2.2 Å resolution, respectively, using the Se-methionine-based multiple anomalous dispersion method for initial phase determination. The structures of apo-HmdII and reconstituted holo-HmdII are almost identical. Like Hmd, HmdII is a homodimer composed of a C-unit formed by the intertwined C-terminal segments (residues 205–355) of the two subunits and two N-units both binding one FeGP cofactor (residues 1–204) [3]. Despite related global architectures reflected in an rmsd of 2.9 Å (271 of 353 residues), HmdII and Hmd reveal remarkable structural changes (Fig. 3A,B) of potential functional relevance.

The structure of the loop region after the strand 13 : 17 directly involved in the FeGP cofactor binding is largely conserved, but adjacent regions that pack against it as the two-helical segment (residues 22–40) and the helical region (residues 68–115) of Hmd are truncated in HmdII. Apparently, the FeGP cofactor binding site is more loosely anchored with the rest of the protein in HmdII than in Hmd.

The C terminus of each subunit is prolonged in HmdII by ~ 50 residues (residues 302–353) compared with Hmd. This dominantly helical segment increases not only the interface between the C-terminal segments of both subunits, but also the interface between the C- and N-units. Helix 336 : 351 contacts helix 131 : 140, and residues 315–319 the loop after strand 167 : 171, whose prolongation of nine residues in HmdII affords this contact. Consequently, the transition between open and closed states, as postulated for Hmd [2,3,25] might be impaired in HmdII. In addition, the rigid-body movement of the N-unit relative to the C-unit is much smaller between apo- and holo-HmdII than between apo- and holo-Hmd. In principle, this finding supports the limited open-to-close capabilities but might also be triggered by crystal lattice effects. Interestingly, the conformation of apo- and holo-HmdII structures rather resembles that of the closed apo-Hmd.

We analyzed the charge distribution of the surface of HmdII and Hmd to determine differences between them for identifying potential binding sites for other proteins present in HmdII, but not in Hmd. However, no attractive hot spot on the HmdII surface could be identified. A positively charged patch was detectable around the binding site of the FeGP cofactor in

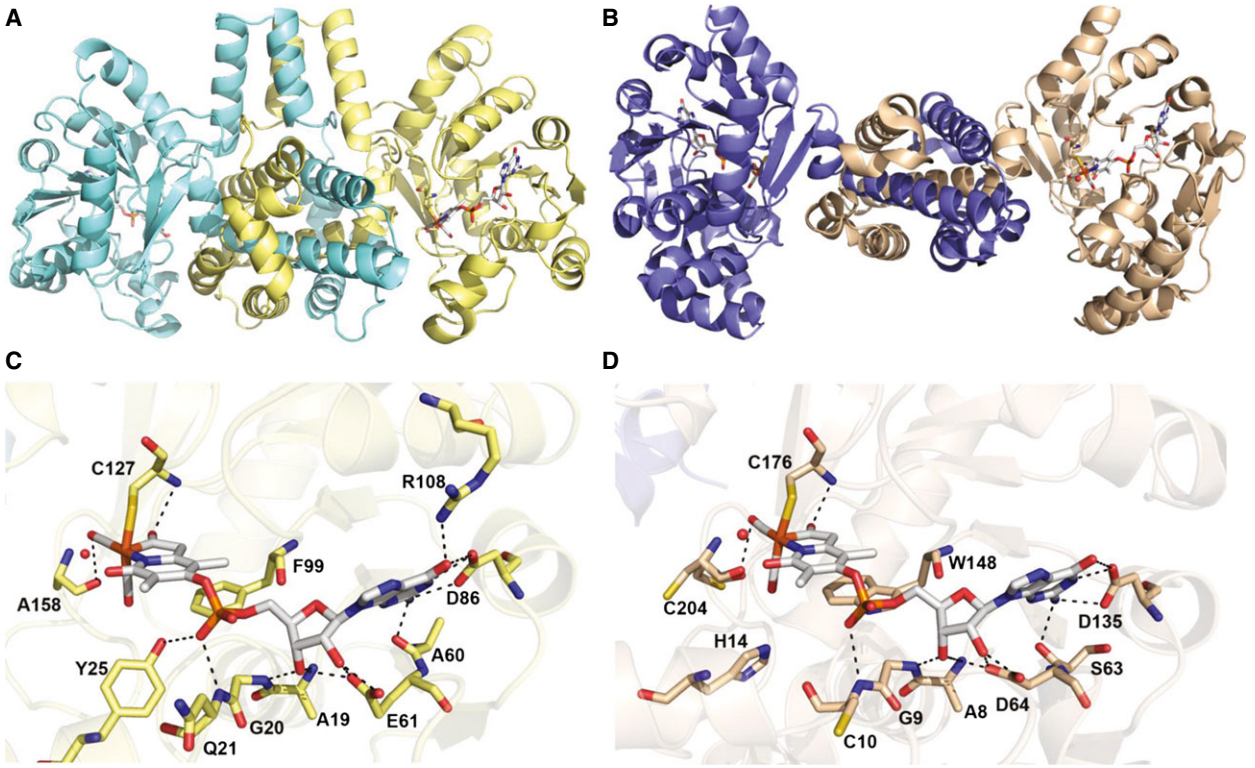

Fig. 3. X-Ray crystal structure of (A) holo-HmdII and (B) holo-Hmd, both from *Methanocaldococcus jannaschii* [1,2]. The FeGP cofactor is represented as a gray stick model. (C) FeGP cofactor binding site in holo-HmdII. (D) FeGP cofactor binding site in holo-Hmd. Residues in contact to the FeGP cofactor are represented as yellow and wheat stick models, respectively. Polar interactions are shown as black dashed lines.

apo-Hmd and even more extended in apo-HmdII (data not shown), which was partly neutralized after FeGP binding.

Binding of the FeGP cofactor

FeGP cofactor is bound in holo-HmdII at the same position and in a related conformation as in holo-Hmd (Fig. 3C,D). Several cofactor–protein interactions, i.e. Cys127 to Fe as well as Asp86 and Glu61 (HmdII nomenclature) to guanosine, conserved between HmdII and Hmd argue for HmdII as a natural FeGP cofactor binding protein. Nevertheless, notable differences exist. The pyridinol ring is sandwiched between Phe99 and Phe102 in HmdII and by the more polar Trp148 and Lys151 in Hmd. Trp148 forms, in addition, a hydrogen bond to the phosphate group of the FeGP cofactor, which is compensated by a hydrogen bond with Tyr25 in HmdII. Tyr25 is replaced by His14 in Hmd, which possibly serves as an acceptor for the proton released after heterolytic cleavage of H_2; substitution of His14 with alanine in Hmd leads to a dramatic decrease in enzymatic activity [2,4].

Methylene-H_4MPT binding to apo-HmdII

Crystals of apo-HmdII were soaked with methenyl-H_4MPT$^+$ and methylene-H_4MPT and their structures were determined by the molecular replacement method (Table 1). In contrast to methenyl-H_4MPT$^+$, methylene-H_4MPT could be bound to apo-HmdII with a high occupancy. Extra electron density interpretable as methylene-H_4MPT was clearly visible in the active site cleft next to Cys127, a ligand of the FeGP cofactor iron in holo-HmdII (Fig. 4). Its conformation resembles that of methylene-H_4MPT bound to holo-Hmd C176A (PDB code 3H65) (Fig. 4D) [2]. In both Hmd and HmdII, the electron density of methenyl-H_4MPT after the benzyl group is weak and beyond the ribose group is largely blurred [2]. In HmdII, the pterin ring of methylene-H_4MPT of apo-HmdII forms polar interactions with Ala212, Ser216 and Ser279, the latter residue originates from the counter monomer (Fig. 4C). In addition, methylene-H_4MPT is flanked by several nonpolar and well-distributed residues including Leu24, Tyr25, Val159, Met214, Ile237, Ala239, Met243 and Met283, suggesting that its binding to HmdII has a biological function. Moreover,

Table 1. Data collection and refinement statistics.

	SeMet-apo-HmdII (MAD peak)	SeMet-apo-HmdII (MAD inflection)	SeMet-apo-HmdII (MAD remote)	SeMet-apo-HmdII (For refinement)	apo-HmdII	HmdII with bound FeGP cofactor	SeMet-HmdII with bound methylene-H_4MPT
Data collection							
Temperature (K)	100	100	100	100	100	100	100
Wavelength (Å)	0.9791	0.9798	0.9720	0.9791	1.000	1.000	1.000
Space group	$P2_12_12_1$	$P2_12_12_1$	$P2_12_12_1$	$P2_12_12_1$	$P2_12_12_1$	$P4_12_12$	$P2_12_12_1$
Resolution (Å)	50–2.3 (2.6–2.3)	50–1.9 (2.0–1.9)	50–2.3 (2.6–2.3)	50–1.9 (2.0–1.9)	50–1.65 (1.7–1.65)	50–2.2 (2.3–2.2)	50–1.9 (2.0–1.9)
Cell dimensions							
a, *b*, *c* (Å)	52.6, 78.0, 153.7	52.6, 78.0, 153.7	52.6, 78.0, 153.7	52.6, 78.0, 153.7	52.5, 77.8, 153.5	52.6, 78.0, 153.7	53.0, 78.0, 153.9
α, β, γ (°)	90, 90, 90	90, 90, 90	90, 90, 90	90, 90, 90	90, 90, 90	90, 90, 90	90, 90, 90
Completeness (%)[a]	100.0 (100.0)	99.4 (95.9)	99.7 (99.9)	99.3 (95.7)	99.7 (100.0)	99.5 (96.6)	99.0 (98.7)
R_{sym} (%)[a,b]	11.4 (34.7)	11.9 (90.5)	12.3 (63.1)	7.8 (58.6)	6.4 (56.5)	8.4 (31.5)	5.5 (83.6)
I/σ_I[a]	16.2 (7.7)	7.9 (1.3)	8.6 (2.7)	11.8 (2.2)	12.1 (2.9)	17.1 (3.7)	18.8 (2.9)
Redundancy[a]	5.1 (5.2)	4.4 (3.3)	4.4 (4.6)	5.3 (3.9)	4.9 (5.1)	10.1 (3.2)	5.5 (5.7)
Refinement statistics							
Resolution (Å)				43.6–1.9 (1.94–1.9)	43.5–1.65 (1.71–1.65)	42.8–2.2 (2.3–2.2)	43.8–1.9 (1.94–1.90)
No. monomers/ asymmetric unit				2	2	1	2
No. ligands/ asymmetric unit				1	4	1	3
No. waters/ asymmetric unit				225	320	108	176
R_{work}/R_{free} (%)[c,d]				18.5/21.5 (30.5/37.3)	18.6/22.1 (28.0/32.4)	18.6/22.3 (28.9/32.4)	18.4/21.3 (24.6/29.0)
rmsd bond length (Å)				0.008	0.011	0.014	0.013
rmsd bond angle (°)				1.193	1.362	1.913	1.371

[a] Values in parentheses are for the highest resolution shell.
[b] $R_{sym} = \Sigma\Sigma|I - \langle I\rangle|/\Sigma I$, where I is the intensity of each reflection.
[c] $R_{work} = \Sigma||F_o|-k|F_c||/\Sigma|F_o|$, where F_o and F_c are the observed and calculated structure factor amplitudes, respectively.
[d] R_{free} was calculated as the R_{work} for 5% of the reflections that were not included in the refinement. MAD, multiple anomalous dispersion.

methylene-H_4MPT has many more contacts with the polypeptide in the closed apo-HmdII than in the open holo-Hmd C176A structures (Fig. 4D).

Despite various attempts, crystals of the holo-HmdII–methenyl-H_4MPT$^+$ or the holo-HmdII–methylene-H_4MPT complexes were not obtained. To analyze the arrangement of the FeGP cofactor relative to methylene-H_4MPT, apo-HmdII with bound methylene-H_4MPT and holo-HmdII were superimposed. In the resulting model, the C14a atom of methylene-H_4MPT is placed 2.4 Å from the iron site of the FeGP cofactor (Fig. 4E). Only small rearrangements in the holo-HmdII–methylene-H_4MPT complex are required to provide enough space for H_2 binding and an optimal active site geometry. The obtained FeGP cofactor–methylene-H_4MPT geometry is similar to that proposed for Hmd modeled from the open holo-Hmd C176A–methylene-H_4MPT complex and the apo-Hmd structure (Fig. 4E,F) [2]. The same catalytic capabilities for HmdII and Hmd appear to be conceivable.

Activity assays of holo-HmdII

The recombinantly produced, pure and successfully reconstituted holo-HmdII now allowed serious kinetic studies to find out its catalytic activity. To probe Hmd-like reactions, we assayed the oxidation of methylene-H_4MPT and methylene-tetrahydrofolate (tetrahydrofolate is an analog of H_4MPT), and the reduction of methenyl-H_4MPT$^+$ and methenyl-tetrahydrofolate with H_2 both at 40 °C under the conditions described in the Materials and Methods. Despite repeated attempts using different preparations, we

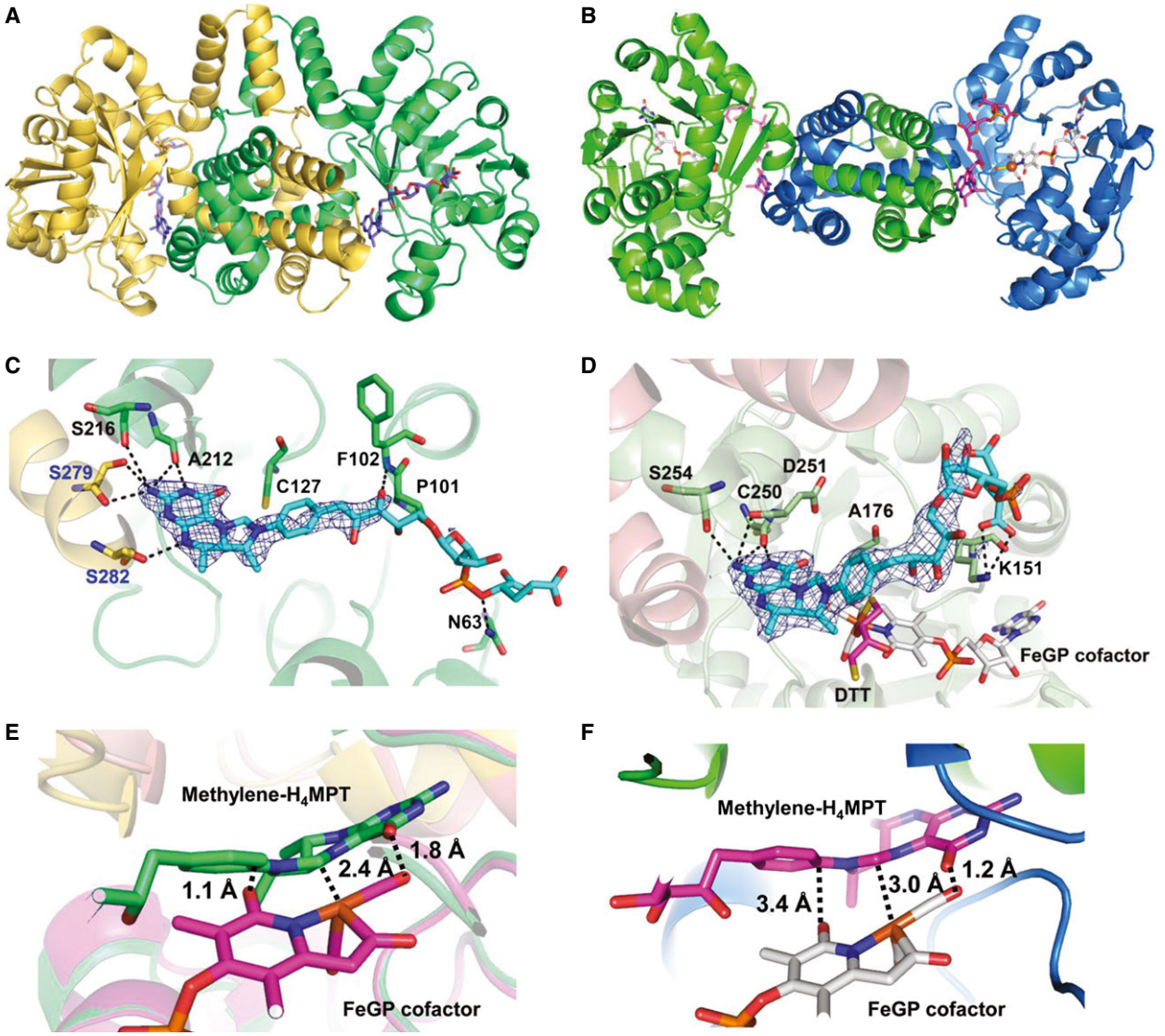

Fig. 4. Crystal structure of apo-HmdII and holo-Hmd C176A with bound methylene-H_4MPT. (A) Structure of apo-HmdII with bound methylene-H_4MPT (purple stick model). (B) Structure of holo-Hmd C176A from *Methanocaldococcus jannaschii* with bound methylene-H_4MPT (violet stick model). (C) Methylene-H_4MPT binding site in apo-HmdII. Amino acid residues with blue labels belong to the partner monomer of the homodimer. The black dashed lines indicate hydrogen bonds between methylene-H_4MPT and the amino acid residues. The $2F_o$–F_c electron density (blue mesh) is contoured at 1σ. (D) Methylene-H_4MPT binding site in holo-Hmd C176A [2]. Hmd and HmdII are shown in the same orientation. (E) Modeled ternary HmdII–FeGP–methylene-H_4MPT–FeGP complex. For modeling apo-HmdII with bound methylene-H_4MPT (magenta and pink cartoons for the two HmdII subunits) and holo-HmdII (green and yellow cartoons) were superimposed. The distances between methylene-H_4MPT and the FeGP cofactor (black dashed lines) are indicated. (F) Modeled ternary Hmd–FeGP–methylene-H_4MPT–FeGP complex. Apo-Hmd and the holo-Hmd C176A–methylene-H_4MPT complex were superimposed [2].

could not detect any catalytic activity of holo-HmdII. Following the proposal of Reeve *et al.* [22], we also tried to measure the reduction of methylene-H_4MPT with H_2 to methyl-H_4MPT. Again, no catalytic activity was found. With the aim of recovering the Hmd activity, an exchange of Tyr25 of HmdII with a histidine was performed because the histidine at this position in Hmd was considered as a proton acceptor after H_2 cleavage [2]. However, the Tyr25His HmdII variant was catalytically inactive.

Previous UV/vis and CD spectroscopic measurements indicated that Hmd with bound methenyl-H_4MPT$^+$ can reversibly accept hydride from H_2 and produce methylene-H_4MPT under single turnover conditions at pH 6.0 [25]. To probe the single turnover Hmd reaction of holo-HmdII at the same conditions,

we used equimolar concentrations (0.1 mM) of enzyme and substrate, but could not detect any activity (data not shown).

Discussion

Over the years, several functional studies on HmdII and HmdIII have been performed. The *hmdII* and *hmdIII* genes are upregulated at low and high concentrations of H_2, respectively [22] when expressed in *Methanothermobacter thermautotrophicus* cells grown under laboratory conditions. Likewise, expression of *hmdII* in *Methanococcus maripaludis* is upregulated under syntrophic growth conditions [26]. The amounts of HmdII and HmdIII in *Methanothermobacter marburgensis* grown under normal conditions are 1% and < 0.1%, respectively, of the soluble proteins in the cell extract based on western blotting [27]. Binding of the FeGP cofactor was predicted by homology models [28] and inhibition of the holoenzyme reconstitution with apo-HmdII [23,24]. HmdII and HmdIII of *M. jannaschii* binds to proyl-tRNA synthetase and tRNA inferred from the copurification of HmdII from cell extracts with prolyl-tRNA synthetase [29,30] and *in vitro* binding studies [31].

Based on this information, various functions for the Hmd-related proteins have been considered: (a) catalytic Hmd isoenzyme [22], (b) H_2 sensor [27], (c) scaffold protein involved in FeGP cofactor biosynthesis [24,28], (d) storage protein for the FeGP cofactor [24,28], and (e) regulation of protein biosynthesis due to the interactions with aminoacyl-tRNA synthetase and tRNA [29–31].

The potential functions for HmdII and HmdIII are predicted based on primary structures, modeled tertiary structures, heterologously produced apoenzymes or cell extracts. The provided pure apo- and holo-HmdII allow a detailed structural and kinetic analysis and open new perspectives for functional studies. Holo-HmdII did not exhibit any catalytic activities with H_4MPT and tetrahydrofolate derivatives and/or H_2 as substrates, despite similar FeGP cofactor and methylene-H_4MPT-binding properties and active site geometries in HmdII and Hmd. A more careful structural inspections reveals two features that rationalizes these findings: (a) the increased interface between N- and C-units, mainly due to a C-terminally prolonged polypeptide chain, impairs the mobility between them which is required for the catalytic cycle of Hmd; and (b) the exchange of a histidine in Hmd to a tyrosine in HmdII. The histidine is most likely involved in proton transfer from buried H_2 to bulk solvent in Hmd [2]. Thus, HmdII is not an isoenzyme or homolog of Hmd but a paralog. We can, of course, not exclude that HmdII uses completely different compounds as substrates but the unambiguous binding of the FeGP cofactor and methylene-H_4MPT does not favor this possibility.

A possible H_2-sensor function of HmdII could be ruled out due to the performed single turnover hydride transfer assays, which exhibited no activity. A single turnover event would be still achievable in the absence of a specific proton uptake and an open-to-closed transition.

Because some methanogenic archaea lack the genes for Hmd paralogs, but still produce active Hmd [20,32] and because *hmdII* gene-deletion experiments with *Methanococcus maripaludis* had no impact on the biosynthesis of the FeGP cofactor [33], a scaffold function for the cofactor biosynthesis can also be ruled out. The affinity between HmdII and methylene-H_4MPT is also not compatible with this idea. The latter argument also makes a storage function of HmdII for the FeGP cofactor unlikely.

The only plausible hypothesis remains a function of HmdII as a regulatory protein in protein synthesis based on the previously found binding of holo-HmdII to aminoacyl-tRNA synthetase and tRNA [29–31]. According to infrared spectroscopic data, HmdII can distinguish between methenyl-H_4MPT$^+$ and methylene-H_4MPT, and binding of the latter induces marked conformational changes around the Fe complex. Therefore, we suggest that HmdII senses the intracellular methylene-H_4MPT concentration, implying that the postulated conformational changes upon methylene-H_4MPT binding alters the affinity of HmdII to potential cellular binding proteins or nucleic acids. Preliminary comparative surface profile analyses of HmdII and Hmd of *M. jannaschii* and protein-docking calculations of HmdII and prolyl-tRNA synthetase from *M. jannaschii* (PDB code: 1NJ8) [34], inconclusive to date, cannot replace future experimental studies. The impact of methylene-H_4MPT on interactions between holo-HmdII and aminoacyl-tRNA synthetases and tRNA (or nucleic acids) has to be biochemically explored. From the perspective of the hydrogenotrophic methanogen, a strict control of protein synthesis under H_2-limiting conditions by the amount of reducing equivalents is beneficial as proposed previously [22]. Methylene-H_4MPT is a metabolite produced in the midst of the methanogenic pathway, and a regulation of protein synthesis by its intracellular concentration would satisfy this need.

We have previously successfully predicted the catalytic function of several proteins based on the crystal structure and on subsequent *in vitro* activity studies

for verification (structure-to-function approach) [35,36]. In this study, structural together with infrared spectroscopic and kinetic data clearly excluded most of the postulated functions of HmdII and we present a hypothesis about its cellular role of methylene-H_4MPT sensor. This hypothesis is consistent with the available data and experimentally verifiable in future on the basis of the established protocol for preparing pure holo-HmdII. This study teaches us that a functional annotation exclusively based on sequence or even convincing structural data still requires a direct experimental validation. Despite similar overall structures, potentially identical prosthetic groups and substrates as well as active site geometries, HmdII is not an Hmd isoenzyme.

Materials and methods

Materials

All chemicals were used without further purification. Poly (ethylene glycol) 300, nickel sulfate, 3- (2-pyridyl)-5,6-di(2-furyl)-1,2,4-triazine-5′5″-disulfonic acid disodium salt (Ferene), and potassium hydroxide were purchased from Sigma-Aldrich (Taufkirchen, Germany). L-Selemomethionine (SeMet) was purchased from Acros Organics (Geel, Belgium). Magnesium chloride, 32% ammonia solution, poly(ethylene glycol) 200 and thiamine were purchased from Merck (Darmstadt, Germany). The following reagents were obtained from Roth (Karlsruhe, Germany): methanol, kanamycin sulfate, ampicillin sodium salt, Mops, imidazole, ammonium chloride, L-methionine, sodium chloride, sodium dihydrogen phosphate, disodium hydrogen phosphate, hydrochloric acid, potassium chloride, potassium dihydrogen phosphate, dipotassium hydrogen phosphate, D-glucose and $FeCl_3{\cdot}6H_2O$. Isopropyl β-D-thiogalactopyranoside was purchased from Fermentas (St. Leon-Rot, Germany).

The FeGP cofactor was isolated from holo-Hmd from *Methanothermobacter marburgensis* [16]. Apo-Hmd was purified from recombinant *Eschericha coli* BL21(DE3) harboring an expression vector, as described previously [8,16]. The expression plasmid with the *M. jannaschii hmdII* gene in pET22b (Novagen, Darmstadt, Germany) at its *Nde*I–*Bam*HI sites was a kind gift of Y.M. Hou [29]. The *M. jannaschii hmdII* Y25H mutant gene with codon optimization for *Escherichia coli* host cells was purchased from GenScript USA Inc. (Piscataway, NJ, USA) as *hmdII* Y25H-pET24b (Novagen). Methenyl-H_4MPT^+ and methylene-H_4MPT were prepared, as reported previously [37]. (6*R*,*S*) -5,10-methenyl-5,6,7,8-tetrahydrofolic acid chloride and (6*R*,*S*) -5,10-methylene-5,6,7,8-tetrahydrofolic acid calcium salt were purchased from Schircks Laboratories (Jona, Switzerland).

Amino acid sequences were aligned using CLUSTAL W2 [38]. The figure of the alignment was generated using ESPRIPT3 [39].

Heterologous production and purification of HmdII

Escherichia coli BL21 (DE3) cells were transformed with the expression plasmid containing *M. jannaschii* apo-HmdII with a C-terminal His_6 tag and grown at 37 °C in Luria–Bertani medium supplemented with 100 $\mu g{\cdot}mL^{-1}$ ampicillin to an optical density 600 (OD600) = 1.0. Protein expression was induced by the addition of 1 mM isopropyl β-D-thiogalactopyranoside. After incubation for 4–6 h the cells were harvested by centrifugation and stored at −80 °C before further use. The apo-HmdII Y25H mutant was produced in the same way as apo-HmdII using 50 $\mu g{\cdot}mL^{-1}$ kanamycin instead of 100 $\mu g{\cdot}mL^{-1}$ ampicillin. All procedures for the purification of apo-HmdII and the apo-HmdII Y25H mutant were performed on ice or at 4 °C. The frozen cells containing apo-HmdII and the apo-HmdII Y25H mutant were resuspended in 50 mM potassium phosphate buffer (pH 7.0) containing 0.5 M KCl, 20 mM imidazole and 1 mM dithiothreitol (buffer A), and disrupted by sonication. The supernatant was collected by centrifugation and loaded onto a Ni^{2+}-charged HiTrap chelating column (GE Healthcare, Uppsala, Sweden) equilibrated with buffer A. The column was washed with buffer A and eluted with a linear gradient of imidazole from 20 to 500 mM in 50 mM potassium phosphate buffer (pH 7.0) containing 0.5 M KCl and 1 mM dithiothreitol. The protein fractions were concentrated with a Centrifugal Filter Unit (Merck Millipore, Darmstadt, Germany) and loaded onto a HiPrep sephacryl S-200 column (GE Healthcare) equilibrated with 50 mM potassium phosphate buffer (pH 7.0) containing 0.3 M KCl and 1 mM dithiothreitol. The purity of the final sample was estimated by SDS/PAGE. Protein concentration was determined by the Bradford method. For the SeMet-labeled apo-HmdII preparation, *E. coli* B834 (DE3) (Novagen) cells transformed with the expression vector carrying the *hmdII* gene were cultured in M9 medium supplemented with 2.5 mM $MgSO_4$, 2% (w/v) D-glucose, 0.01% (w/v) thiamine, 0.025 mM $FeCl_3$, 50 $\mu g{\cdot}mL^{-1}$ L-selenomethionine, and 100 $\mu g{\cdot}mL^{-1}$ ampicillin at 37 °C to an OD600 = 0.5 before induction of expression with 1 mM isopropyl β-D-thiogalactopyranoside as described above. SeMet-apo-HmdII was purified as described for apo-HmdII.

Reconstitution of the holoenzymes

To reconstitute the holoenzymes, apo-HmdII and apo-HmdII Y25H mutant were mixed with the FeGP cofactor under a N_2/H_2 (95%/5%) atmosphere at 8 °C in an anaerobic chamber (Coy Laboratories, Grass Lake, MI, USA) under red or yellow light [16]. The buffers of purified

apo-HmdII and apo-HmdII Y25H mutant were exchanged with anoxic 10 mM Mops/KOH (pH 7.0) buffer containing 1 mM dithiothreitol using a PD-10 column (GE Healthcare). Apo-HmdII and the apo-HmdII Y25H mutant were then incubated with at least 1.5 eq. of the FeGP cofactor in 0.1 M Tris/HCl buffer pH 8.0 for 1 h at 8 °C under anoxic conditions. The mixture of apo-HmdII and apo-HmdII Y25H mutant with FeGP cofactor was loaded onto a PD-10 column equilibrated with 10 mM Mops/KOH buffer containing 1 mM dithiothreitol (pH 7.0) to separate HmdII and the apo-HmdII Y25H mutant both reconstituted with FeGP cofactor from unbound FeGP cofactor.

Infrared spectroscopy

Attenuated total reflection-infrared spectra were recorded using a Bruker VERTEX 70V FTIR spectrometer equipped with an MCT detector. Attenuated total reflection optical configuration (DuraSampleIR™, Sensir Technologies, Watford, UK) was employed with a silicon prism. The measurements were handled under red light to avoid photoinduced decomposition of the FeGP cofactor in the samples. Infrared spectra were continuously recorded with averaging of 512 scans at 4 cm^{-1} resolution under an argon stream; the sample was gradually concentrated on the optical element of the attenuated total reflection unit due to an evaporation of the water solute. The spectrum was chosen when the sample concentration was sufficiently high to resolve the CO band from the FeGP cofactor; the water band was subtracted and the spectrum was baseline corrected.

Crystallization

All proteins were crystallized at 8 °C using the sitting drop vapor diffusion method. A 1 μL aliquot of apo-HmdII (12 $mg{\cdot}mL^{-1}$) in 50 mM potassium phosphate buffer (pH 7.0) with 0.3 M KCl was mixed with 1 μL of a reservoir solution composed of 40% (v/v) poly(ethylene glycol) 300 and 100 mM phosphate-citrate buffer (pH 4.2); crystals appeared within 1 week. Crystals of SeMet–apo-HmdII were obtained within 1 week when adding a 1 μL aliquot of SeMet–apo-HmdII (20 $mg{\cdot}mL^{-1}$) in 10 mM Mops/KOH buffer (pH 7.0)/1 mM dithiothreitol to 1 μL of a reservoir solution composed of 35% (v/v) poly(ethylene glycol) 300 and 100 mM phosphate-citrate buffer (pH 4.2). For crystallization of HmdII reconstituted with the FeGP cofactor, all procedures were carried out in a Coy chamber with a N_2/H_2 (95%/5%) atmosphere under red or yellow light. An 1 μL aliquot of HmdII reconstituted with the FeGP cofactor (9 $mg{\cdot}mL^{-1}$) in anoxic 10 mM Mops/KOH buffer (pH 7.0)/1 mM dithiothreitol was mixed with 1 μL of a reservoir solution composed of 50% (v/v) poly(ethylene glycol) 200, 100 mM Na/K-phosphate buffer (pH 6.2), and 0.2 M NaCl. Crystals of HmdII reconstituted with the FeGP cofactor were obtained in a month. SeMet-apo-HmdII crystals were incubated in 0.1 M phosphate-citrate buffer (pH 4.2) containing 34% (v/v) poly(ethylene glycol) 300 and 1.4 mM methenyl-H_4MPT^+ or 1.4 mM methylene-H_4MPT at 8 °C for 1 day.

X-ray data collection and refinement

Crystals of apo-HmdII, SeMet–apo-HmdII, HmdII reconstituted with the FeGP cofactor and SeMet–apo-HmdII incubated with various ligands were frozen under a cryostream of N_2 at 100 K without adding a cryoprotectant. Diffraction data were collected at 100 K on beamline X10SA equipped with a PILATUS 6M detector at the Swiss Light Source (Villigen, Switzerland). Data were processed using XDS [40]. To determine the crystal structure of apo-HmdII, multiple anomalous dispersion data were measured at the selenium edge of the SeMet–apo-HmdII crystals. Selenium atom sites were detected with SHELX C/D [41]. Phases were determined using the program SHARP and improved by the solvent flattening procedure of SOLOMON implemented in SHARP [42]. Automated model building was performed using ARP/WARP [43]. The SeMet–apo-HmdII model was manually completed and refined using COOT [44], REFMAC5 [45] and PHENIX [46]. Crystal structures of other crystal forms of HmdII were solved by molecular replacement with MOLREP [47] or PHASER [48] using the SeMet–apo-HmdII structure as a search model. The TLS option was used for all structures in the final stage of refinement [49]. The final models were validated using MOLPROBITY [50]. The resulting structures were established at a resolution of 1.7 Å for apo-HmdII, 1.9 Å for SeMet–apo-HmdII, 2.2 Å for holo-HmdII, 1.9 Å for methylene-H_4MPT-bound SeMet–apo-HmdII, and 1.9 Å for methenyl-H_4MPT^+-bound SeMet-apo-HmdII. Data collection and refinement statistics are summarized in Table 1. Atomic coordinates and structure factors are available in the Protein Data Bank (www.pdb.org) under the accession numbers; 4YT8 for SeMet-labeled apo-HmdII; 4YT2 for apo-HmdII; 4YT4 for holo-HmdII; 4YT5 for apo-HmdII with bound methylene-H_4MPT. Crystal structures were superimposed using DALILITE [51] or SUPERPOSE [52] in CCP4 [53]. Charge distributions on the surfaces of the structures were calculated by PYMOL (v. 1.3r1, Schrödinger, LLC). Figures 3 and 4 were generated by PYMOL (v. 1.3r1, Schrödinger, LLC).

Enzyme activity assay

To assay the conversion of methenyl-H_4MPT^+ to methylene-H_4MPT, holo-HmdII or the holo-HmdII Y25H mutant was added to 20μM methenyl-H_4MPT^+ in 120 mM potassium phosphate buffer (pH 7.5) in a 1-cm-path quartz cuvette under 100% H_2 at 40 °C. To assay Hmd-catalyzed conversion of methylene-H_4MPT to methenyl-H_4MPT^+, holo-HmdII or the holo- HmdII Y25H mutant was added

to 20μM methylene-H_4MPT in 120 mM potassium phosphate buffer (pH 6.0) inside a 0.3-cm-path quartz cuvette under 100% N_2. Methenyl-tetrahydrofolate and methylene-tetrahydrofolate were tested as the Hmd-catalyzed reactions described above. The change in absorbance at 336 nm was monitored. For the activity under single-turn-over conditions, UV/vis spectra of 0.1 mM HmdII in 50 mM Mes/NaOH (pH 6.0) in the presence of 0.1 mM methenyl-H_4MPT^+ under N_2, and H_2 were measured as described previously [25].

Acknowledgements

We thank Prof. Dr Rolf Thauer for discussions and helpful suggestions, Prof. Dr Hartmut Michel for continuous support, and the staff of the PXII beamline at the Swiss Light Source (Villigen) and Ulrike Demmer for help during data collection and X-ray structure analysis. We thank Prof. Ya-Ming Hou for kindly providing the expression plasmid for *M. jannaschii* HmdII. This work was supported by a grant of the Max Planck Society to R. Thauer and a grant of the PRESTO program from the Japan Science and Technology Agency to SS.

Author contributions

SS directed the research. TF and SS designed the research. TF prepared, crystallized and characterized proteins. KA performed the infrared spectroscopy. TF and UE performed the X-ray crystallographic analysis. TF, UE and SS interpreted the data and wrote the manuscript.

References

1 Hiromoto T, Ataka K, Pilak O, Vogt S, Stagni MS, Meyer-Klaucke W, Warkentin E, Thauer RK, Shima S & Ermler U (2009) The crystal structure of C176A mutated [Fe] -hydrogenase suggests an acyl- iron ligation in the active site iron complex. *FEBS Lett* **583**, 585–590.

2 Hiromoto T, Warkentin E, Moll J, Ermler U & Shima S (2009) The crystal structure of an [Fe] -hydrogenase-substrate complex reveals the framework for H_2 activation. *Angew Chem Int Ed* **48**, 6457–6460.

3 Pilak O, Mamat B, Vogt S, Hagemeier CH, Thauer RK, Shima S, Vonrhein C, Warkentin E & Ermler U (2006) The crystal structure of the apoenzyme of the iron-sulphur cluster-free hydrogenase. *J Mol Biol* **358**, 798–809.

4 Shima S, Pilak O, Vogt S, Schick M, Stagni MS, Meyer-Klaucke W, Warkentin E, Thauer RK & Ermler U (2008) The crystal structure of [Fe] -hydrogenase reveals the geometry of the active site. *Science* **321**, 572–575.

5 Lubitz W, Ogata H, Rudiger O & Reijerse E (2014) Hydrogenases. *Chem Rev* **114**, 4081–4148.

6 Shima S & Ermler U (2011) Structure and function of [Fe] -hydrogenase and its iron-guanylylpyridinol (FeGP) cofactor. *Eur J Inorg Chem* **2011**, 963–972.

7 Thauer RK, Kaster AK, Goenrich M, Schick M, Hiromoto T & Shima S (2010) Hydrogenases from methanogenic archaea, nickel, a novel cofactor, and H_2 storage. *Annu Rev Biochem* **79**, 507–536.

8 Buurman G, Shima S & Thauer RK (2000) The metal-free hydrogenase from methanogenic archaea: evidence for a bound cofactor. *FEBS Lett* **485**, 200–204.

9 Korbas M, Vogt S, Meyer-Klaucke W, Bill E, Lyon EJ, Thauer RK & Shima S (2006) The iron-sulfur cluster-free hydrogenase (Hmd) is a metalloenzyme with a novel iron binding motif. *J Biol Chem* **281**, 30804–30813.

10 Lyon EJ, Shima S, Boecher R, Thauer RK, Grevels FW, Bill E, Roseboom W & Albracht SPJ (2004) Carbon monoxide as an intrinsic ligand to iron in the active site of the iron-sulfur-cluster-free hydrogenase H_2-forming methylenetetrahydromethanopterin dehydrogenase as revealed by infrared spectroscopy. *J Am Chem Soc* **126**, 14239–14248.

11 Shima S, Lyon EJ, Sordel-Klippert MS, Kauss M, Kahnt J, Thauer RK, Steinbach K, Xie XL, Verdier L & Griesinger C (2004) The cofactor of the iron-sulfur cluster free hydrogenase Hmd: structure of the light-inactivation product. *Angew Chem Int Ed* **43**, 2547–2551.

12 Shima S, Lyon EJ, Thauer RK, Mienert B & Bill E (2005) Mössbauer studies of the iron-sulfur cluster-free hydrogenase: the electronic state of the mononuclear Fe active site. *J Am Chem Soc* **127**, 10430–10435.

13 Shima S, Schick M, Kahnt J, Ataka K, Steinbach K & Linne U (2012) Evidence for acyl-iron ligation in the active site of [Fe] -hydrogenase provided by mass spectrometry and infrared spectroscopy. *Dalton Trans* **41**, 767–771.

14 Shima S & Ataka K (2011) Isocyanides inhibit [Fe] -hydrogenase with very high affinity. *FEBS Lett* **585**, 353–356.

15 Tamura H, Salomone-Stagni S, Fujishiro T, Warkentin E, Meyer-Klaucke W & Ermler U (2013) Crystal structures of [Fe] -hydrogenase in complex with inhibitory isocyanides: implications for H2-activation site. *Angew Chem Int Ed* **52**, 9656–9659.

16 Shima S, Schick M & Tamura H (2011) Preparation of [Fe] -hydrogenase from methanogenic archaea. *Method Enzymol* **494**, 119–137.

17 Smith DR, DoucetteStamm LA, Deloughery C, Lee HM, Dubois J, Aldredge T, Bashirzadeh R, Blakely D, Cook R, Gilbert K *et al.* (1997) Complete genome sequence of *Methanobacterium thermoautotrophicum* ΔH: functional analysis and comparative genomics. *J Bacteriol* **179**, 7135–7155.

18 Bult CJ, White O, Olsen GJ, Zhou LX, Fleischmann RD, Sutton GG, Blake JA, FitzGerald LM, Clayton RA, Gocayne JD *et al.* (1996) Complete genome sequence of the methanogenic archaeon, *Methanococcus jannaschii*. *Science* **273**, 1058–1073.
19 Samuel BS, Hansen EE, Manchester JK, Coutinho PM, Henrissat B, Fulton R, Latreille P, Kim K, Wilson RK & Gordon JI (2007) Genomic and metabolic adaptations of *Methanobrevibacter smithii* to the human gut. *Proc Natl Acad Sci USA* **104**, 10643–10648.
20 Schwörer B & Thauer RK (1991) Activities of formylmethanofuran dehydrogenase, methylenetetrahydromethanopterin dehydrogenase, methylenetetrahydromethanopterin reductase, and heterodisulfide reductase in methanogenic bacteria. *Arch Microbiol* **155**, 459–465.
21 Goker M, Daligault H, Mwirichia R, Lapidus A, Lucas S, Deshpande S, Pagani I, Tapia R, Cheng JF, Goodwin L *et al.* (2011) Complete genome sequence of the thermophilic sulfur-reducer *Desulfurobacterium thermolithotrophum* type strain (BSA^T) from a deep-sea hydrothermal vent. *Stand Genomic Sci* **5**, 407–415.
22 Reeve JN, Nölling J, Morgan RM & Smith DR (1997) Methanogenesis: genes, genomes, and who's on first? *J Bacteriol* **179**, 5975–5986.
23 Pilak O (2004) Synthese von Hydrogenase Hmd und von zwei vermuteten Isoenzymen in *Methanothermobacter marburgensis* bei Wachstum unter Fe-, NH_3-oder Ni-Limitierung, *Diplomarbeit Phillipps-Universität Marburg*.
24 Shima S & Thauer RK (2007) A third type of hydrogenase catalyzing H_2 activation. *Chem Rec* **7**, 37–46.
25 Shima S, Vogt S, Gobels A & Bill E (2010) Iron-chromophore circular dichroism of [Fe] -hydrogenase: the conformational change required for H_2 activation. *Angew Chem Int Ed* **49**, 9917–9921.
26 Walker CB, Redding-Johanson AM, Baidoo EE, Rajeev L, He ZL, Hendrickson EL, Joachimiak MP, Stolyar S, Arkin AP, Leigh JA *et al.* (2012) Functional responses of methanogenic archaea to syntrophic growth. *ISME J* **6**, 2045–2055.
27 Afting C, Kremmer E, Brucker C, Hochheimer A & Thauer RK (2000) Regulation of the synthesis of H_2-forming methylenetetrahydromethanopterin dehydrogenase (Hmd) and of HmdII and HmdIII in *Methanothermobacter marburgensis*. *Arch Microbiol* **174**, 225–232.
28 Goldman AD, Leigh JA & Samudrala R (2009) Comprehensive computational analysis of Hmd enzymes and paralogs in methanogenic archaea. *BMC Evol Biol* **9**, 199.
29 Lipman RSA, Chen J, Evilia C, Vitseva O & Hou YM (2003) Association of an aminoacyl-tRNA synthetase with a putative metabolic protein in archaea. *Biochemistry* **42**, 7487–7496.
30 Lipman RSA, Sowers KR & Hou YM (2000) Synthesis of cysteinyl-tRNA(Cys) by a genome that lacks the normal cysteine-tRNA synthetase. *Biochemistry* **39**, 7792–7798.
31 Oza JP, Sowers KR & Perona JJ (2012) Linking energy production and protein synthesis in hydrogenotrophic methanogens. *Biochemistry* **51**, 2378–2389.
32 Schick M, Xie XL, Ataka K, Kahnt J, Linne U & Shima S (2012) Biosynthesis of the iron-guanylylpyridinol cofactor of [Fe] -Hydrogenase in methanogenic archaea as elucidated by stable-isotope labeling. *J Am Chem Soc* **134**, 3271–3280.
33 Lie TJ, Costa KC, Pak D, Sakesan V & Leigh JA (2013) Phenotypic evidence that the function of the [Fe] -hydrogenase Hmd in *Methanococcus maripaludis* requires seven *hcg* (*hmd* co-occurring genes) but not *hmdII*. *FEMS Microbiol Lett* **343**, 156–160.
34 Kamtekar S, Kennedy WD, Wang JM, Stathopoulos C, Soll D & Steitz TA (2003) The structural basis of cysteine aminoacylation of tRNA(Pro) by prolyl-tRNA synthetases. *Proc Natl Acad Sci USA* **100**, 1673–1678.
35 Fujishiro T, Kahnt J, Ermler U & Shima S (2015) Protein-pyridinol thioester precursor for biosynthesis of the organometallic acyl-iron ligand in [Fe] -hydrogenase cofactor. *Nat Commun* **6**, 6895.
36 Fujishiro T, Tamura H, Schick M, Kahnt J, Xie XL, Ermler U & Shima S (2013) Identification of the HcgB enzyme in [Fe] -hydrogenase-cofactor biosynthesis. *Angew Chem Int Ed* **52**, 12555–12558.
37 Shima S & Thauer RK (2001) Tetrahydromethanopterin-specific enzymes from *Methanopyrus kandleri*. *Methods Enzymol* **331**, 317–353.
38 Larkin MA, Blackshields G, Brown NP, Chenna R, McGettigan PA, McWilliam H, Valentin F, Wallace IM, Wilm A, Lopez R *et al.* (2007) Clustal W and clustal X version 2.0. *Bioinformatics* **23**, 2947–2948.
39 Robert X & Gouet P (2014) Deciphering key features in protein structures with the new ENDscript server. *Nucleic Acids Res* **42**, W320–W324.
40 Kabsch W (2010) Xds. *Acta Crystallogr D* **66**, 125–132.
41 Sheldrick GM (2008) A short history of SHELX. *Acta Crystallogr A* **64**, 112–122.
42 dela Fortelle E & Bricogne G (1997) Maximum-likelihood heavy-atom parameter refinement for multiple isomorphous replacement and multiwavelength anomalous diffraction methods. *Methods Enzymol* **276**, 472–494.
43 Langer G, Cohen SX, Lamzin VS & Perrakis A (2008) Automated macromolecular model building for X-ray crystallography using ARP/wARP version 7. *Nat Protoc* **3**, 1171–1179.

44 Emsley P & Cowtan K (2004) Coot: model-building tools for molecular graphics. *Acta Crystallogr D* **60**, 2126–2132.
45 Murshudov GN, Vagin AA & Dodson EJ (1997) Refinement of macromolecular structures by the maximum-likelihood method. *Acta Crystallogr D* **53**, 240–255.
46 Afonine PV, Grosse-Kunstleve RW, Chen VB, Headd JJ, Moriarty NW, Richardson JS, Richardson DC, Urzhumtsev A, Zwart PH & Adams PD (2010) *phenix.model_vs_data:* a high-level tool for the calculation of crystallographic model and data statistics. *J Appl Crystallogr* **43**, 669–676.
47 Vagin A & Teplyakov A (1997) MOLREP: an automated program for molecular replacement. *J Appl Crystallogr* **30**, 1022–1025.
48 Mccoy AJ, Grosse-Kunstleve RW, Adams PD, Winn MD, Storoni LC & Read RJ (2007) Phaser crystallographic software. *J Appl Crystallogr* **40**, 658–674.
49 Winn MD, Isupov MN & Murshudov GN (2001) Use of TLS parameters to model anisotropic displacements in macromolecular refinement. *Acta Crystallogr D* **57**, 122–133.
50 Chen VB, Arendall WB, Headd JJ, Keedy DA, Immormino RM, Kapral GJ, Murray LW, Richardson JS & Richardson DC (2010) MolProbity: all-atom structure validation for macromolecular crystallography. *Acta Crystallogr D* **66**, 12–21.
51 Holm L, Kaariainen S, Rosenstrom P & Schenkel A (2008) Searching protein structure databases with DaliLite v. 3. *Bioinformatics* **24**, 2780–2781.
52 Krissinel E & Henrick K (2004) Secondary-structure matching (SSM), a new tool for fast protein structure alignment in three dimensions. *Acta Crystallogr D* **60**, 2256–2268.
53 Winn MD, Ballard CC, Cowtan KD, Dodson EJ, Emsley P, Evans PR, Keegan RM, Krissinel EB, Leslie AGW, McCoy A *et al.* (2011) Overview of the CCP4 suite and current developments. *Acta Crystallogr D* **67**, 235–242.